JAAS

ROYAL SOCIETY OF CHEMISTRY

PAPER

View Article Online
View Journal

Cite this: DOI: 10.1039/d5ja00350d

Towards improved workflows for the production and metrological characterization of LA-ICP-MS calibration standards for quantitative bioimaging

Kharmen Billimoria, [a] Paula Menero-Valdes, *[a] William Lee, [b] Alex Shard [b] and Heidi Goenaga Infante [a]

The lack of suitable calibration standards is a persistent bottleneck for quantitative bioimaging by LA-ICP-MS. Widespread use of in-house calibration approaches has led to a lack of harmonisation limiting the potential of LA-ICP-MS in clinical or biomedical fields. This work addresses this challenge by utilising automation *via* a bioprinting approach to produce re-usable gelatin-droplet standards, doped with multiple elements for both instrument tuning and quantitative analysis. The resulting standards were systematically characterized in terms of thickness, elemental homogeneity, and long-term stability. Droplets were doped with Ti, Ce, Au, Th and U (used for instrument tuning) as well as increasing concentrations of lanthanides such as Gd and Yb (typically used in bio-clinical applications). Variation of thickness (measured by ellipsometry) between droplets, after printing and dehydration, was 5% (RSD, $n = 12$). Intra- and inter-droplet elemental homogeneity were less than 6% (RSD, $n = 10$) and 8% (RSD, $n = 9$), respectively for all elements. Due to the reproducibility of both physical characteristics (thickness and size) and elemental distribution, there is no need of ablating the entire droplet. Instead, ablation of an area as small as 1 line across a droplet produced elemental data which is representative of the entire droplet. This feature enables the same droplet to be used across multiple batches or multiple times within a batch, the latter for quality control purposes. Data from long-term stability and shipping tests highlight the usability of these standards and a potential route towards harmonisation.

Received 8th September 2025
Accepted 20th November 2025

DOI: 10.1039/d5ja00350d

rsc.li/jaas

Introduction

The LA-ICP-MS imaging has significantly advanced in the past years; mainly due to instrumentation development which has enabled faster acquisition times of high-resolution maps with greater sensitivity. As demonstrated in recently published work by Basabe-Mendizabal *et al.*,[1] using a novel low-dispersion ablation cell design has made the acquisition of maps at 1000 pixels s^{-1} possible. However, despite the technological progress, many bioimaging applications remain semiquantitative, reliant on in-house calibration standards due to the lack of well-characterized biomaterials that can be used for quantification.[2]

[a]National Measurement Laboratory, LGC, 10 Priestley Rd, Guildford, GU2 7XY, UK. E-mail: paula.menerovaldes@lgcgroup.com

[b]National Physical Laboratory, Hampton Road, Teddington, TW11 0LW, UK

Paula Menero-Valdes

Dr Paula Menero-Valdés is a researcher at the National Measurement Laboratory (NML) at LGC, working within the Inorganic Analysis Team. She earned her PhD in Analytical Chemistry cum laude from the University of Oviedo (Spain) in 2024, under the supervision of Prof. Rosario Pereiro and Dr Beatriz Fernández. Her doctoral research focused on the use of metallic nanoclusters as elemental tags for mass spectrometric studies of proteins associated with ocular neurodegenerative diseases, in collaboration with clinicians at the Fernández Vega Ophthalmological Institute (Oviedo, Spain). During her PhD, she carried out a research stay in Division 1.1 at BAM (Berlin) with Dr Björn Meermann, where she began exploring ICP ToF-MS for single-cell population studies. In September 2024 she joined the NML, her research addresses metrological challenges in imaging LA-ICP-MS and single-cell ICP-MS, with an emphasis on pushing the limits of quantification in biological systems. Her work has been presented at numerous international conferences, and she has co-chaired a session at the 2025 SciX conference (USA). She received the 2024 SAS Atomic Student Award and has authored over ten publications in leading Q1 journals. In addition, she is actively engaged in science outreach, giving lectures to school students and organizing the II PhD Multichemical Congress (Gijón, Spain, 2024).

The absence of a harmonised calibration strategy limits data comparability across experiments or between laboratories. This limitation is particularly critical for clinical applications, where absolute quantification enables meaningful comparisons across diseases, patients, and time points (*e.g.*, between *in vivo* and *post-mortem* samples), which is invaluable for making informed decisions for future disease prevention, diagnosis, and treatment. Moreover, as multi-centre and multi-hospital studies involving large patient cohorts continue to grow in relevance, the ability to generate comparable data becomes even more important. Therefore, establishing robust and standardized calibration protocols is vital for LA-ICP-MS imaging applications to be implemented as a reliable tool to support clinical diagnosis and decision-making.

Ideally, for quantitative analysis, certified reference materials (CRMs) are used to generate calibration curves or act as quality control (QC) materials. For example, NIST 61X series of glass materials have been widely adopted in LA-ICP-MS for a variety of geological applications[3,4] due to their elemental homogeneity, stability, reusability, the wide range of elements and their concentration range, making them convenient calibration materials. LA-ICP-MS suffers from matrix effects due to changes in size and geometry of the generated aerosol between standards and samples as well as aerosol transport and ionization in the ICP.[5,6] Therefore, it is vital to choose a calibration standard which has similar chemical, mechanical and optical properties to the sample, to obtain accurate quantitative results.[7] Although there is an increasing number of available matrix-matched geological CRMs for LA-ICP-MS, to date, there is a limited number of CRMs for biological samples available, and are usually presented as powders, which is not ideal for LA-ICP-MS tissue imaging.[8]

Numerous calibration approaches for LA-ICP-MS have been proposed such as strategies based on internal standardization,[9,10] isotope dilution[11] and external calibration,[12] with the latter being the most widely adopted approach.[13] The first attempts to produce a matrix matched external calibration for LA-ICP-MS bioimaging involved the use of spiked homogenised tissue.[14,15] Later, easier to handle matrix-matched materials like polymers[16,17] and gelatin[18,19] were applied to obtain calibration standards. A recent study by Becker *et al.* proposes a process for tissue fossilization prior to LA-ICP-MS analysis, enabling internal standardisation quantification using glass materials such as the NIST 61X series.[20] While this approach helps overcome biases due to differences in ablation rates between sample and calibrant, its implementation as universal approach for quantitative bioimaging using LA-ICP-MS may be limited by incompatibility with certain laser wavelengths (such as 266 nm) that are commonly used in bioimaging applications.

Gelatin remains the most widely adopted matrix of choice to prepare calibration standards for bioimaging applications, as it avoids the handling of biohazardous material while still consisting of a tissue-like matrix, with similar protein content and UV laser interaction.[21] Furthermore, with the incorporation of technologies such as bioprinters and droplet arrayers, new approaches for calibration standard production have evolved from tedious manual protocols to more reproducible and automated time saving workflows.[22]

Automated strategies to produce calibration standards remove some of the more tedious steps for preparing a calibration material whilst also help improve reproducibility and limiting physical variations between standards. Different automated techniques have been evaluated, such as spin-coating[23] and ink-jet printing[24] used to produce thin layer standards or micro-spotting[25] and bioprinting[26] to produce droplet standards. Schweikert *et al.* proposed a multi-element calibration approach with deposited gelatin microdroplets (of approximately 200 μm diameter and 400 pL volume) which are fully ablated during analysis, so that the total mass of analyte per droplet per droplet correlates to the recorded elemental intensities.[27] This calibration approach was then further developed to quantify multiple elements in a single analysis, while also providing semiquantitative data for many others.[28] Previous work also highlighted the benefits of using bioprinting technology to produce re-usable gelatin micro-droplets doped with nanoparticles containing a few elements that showed comparable or better performance than cryo-sectioned gelatin,[26] while significantly reducing the preparation time.

In this study, an improved workflow is proposed for the production and metrological characterization of multi-elemental bioprinted gelatin droplets with an extended suite of elements typically use for instrument optimisation and, calibration in biological applications. To achieve this, gelatin was doped with Ti, Ce and Au nanoparticles (NP) to monitor the sensitivity across the low, mid and high mass to charge ratio (m/z) range, as well as U and Th ionic solutions to assess oxide formation and monitor laser induced fractionation, using ICP-ToF-MS detection. Additionally increasing concentrations of Gd and Yb, in the form of lanthanide carbon dots (LnCDs) were spiked into the gelatin as elements of interest for quantification. Nanoparticles were selected, not only to facilitate homogenous elemental distribution throughout the gelatin droplets but also due to their optical properties, enabling complementary detection by absorbance or fluorescence spectroscopy. The latter extends the applicability of these standards materials to bioimaging techniques other than LA-ICP-MS. The droplet thickness, which is a key parameter for quantification using LA-ICP-ToF-MS, was determined by ellipsometry. Moreover, elemental homogeneity across the droplet was tested both within and between droplets. Information on the within droplet homogeneity was used to assess their feasibility for re-use in multiple calibration batches. This was done by defining the minimum representative area (using the defined imaging parameters) that needs to be ablated per droplet to achieve elemental data that is representative of the entire droplet without sacrifice in performance characteristics. Finally, to investigate whether this preparation strategy has the potential for wider dissemination and interlaboratory comparisons, long term storage and shipment stability were also assessed.

Experimental

Materials and reagents

Gelatin from porcine skin (300 bloom, Merck, UK) was used to prepare the calibration standards. LGCQC5050 Au NPs (LGC

Standards, UK), TiO_2 NPs (NM-100, JRC, Italy), CeO_2NPs (25 nm, 10 wt% in H_2O, Merck, Germany), high purity inorganic stock solutions of U (984.3 μg g^{-1}, Romil, UK), and Th (981.5 μg g^{-1}, Romil, UK) were all purchased and used without modification to spike the gelatin. $GdCl_3 \cdot 6H_2O$ (99.9% trace metals basis, Sigma-Aldrich, Germany), $YbCl_3 \cdot 6H_2O$ (99.9% trace metals basis, Sigma-Aldrich, Germany), citric acid monohydrate (99.5–100.5%, Sigma-Aldrich, Germany) and ammonium citrate dibasic (≥98%, Sigma-Aldrich, Germany) were used as precursors for the synthesis of LnCDs which were used to dope the gelatin solutions.[29] Pur-A-Lyzer cassettes (Sigma-Aldrich, Germany) with 1 kDa pore size and 0.22 μm PVDF membrane filters were used for LnCDs purification. A detailed procedure for the synthesis of the LnCDs can be found in SI. For total elemental analysis using ICP-MS all working solutions were prepared from high purity single element stock solutions (UpA, Romil, Cambridge, UK).

Preparation of bioprinted gelatin calibration standards

A detailed procedure for bioprinting has been previously discussed.[25] Briefly, gelatin (1% w/w) was dissolved in ultrapure water (18.2 MΩ cm, ELGA, UK) at 45 °C and spiked with aliquots of the NP or elemental solutions and mixed well. This gelatin solution was transferred into syringe cartridges and loaded into the BioX6 bioprinter (CELLINK, Göteborg). The syringe is heated to 37 °C and the printed with glass microscope slide is chilled to 12 °C. The bioprinter was configured to print out an 11 × 5 droplet array using 5 kPa extrusion force for 0.02 s. Once printing was completed the slide is removed from the printer and left to air dry for 24 h in a slide box under controlled laboratory conditions (20 ± 2 °C and 50 ± 5% humidity). After this, the slides are stored at room temperature in an airtight container in the dark. The elemental concentration in the prepared gelatin solutions was determined by solution ICP-MS after acidic digestion (details in ESM).

LA-ICP-ToF-MS imaging analysis

All imaging data was acquired using ImageBIO 266 nm laser ablation system fitted with the Two Vol3 ablation chamber and dual concentric injector (ESL, Bozeman), coupled to ICP-ToF-MS 2R (TOFWERK, Thun). All data was acquired in transient imaging mode using a 22 μm laser spot with 4 μm overlap in both *x* and *y* directions and 50 Hz repetition rate. A laser fluence of 4 J cm^{-2} was used to ensure the whole gelatin thickness was quantitatively ablated. The aerosol particles were transferred to the ICP *via* 0.8 L per min He gas flow, and the analysis was carried out in standard no gas mode. A summary of the LA-ICP-ToF-MS instrumental parameters is shown in Table 1. Data treatment including baseline subtraction and mass shift correction was carried out using TofWare (v 3.2.0) and further image processing and data analysis carried out in iolite[30] (v 4.10.0) and MS Excel (v 2503), respectively.

Ellipsometry measurements

Thickness of the dehydrated gelatin standards were measured using a Woollam (Lincoln, Nebraska, USA) M2000DI spectroscopic ellipsometer with a wavelength range of 190 nm to 1700 nm. Three incidence angles (50°, 55°, 60°) were chosen to span the expected Brewster angle of approximately 55° for the glass slide. Focussing optics were used to reduce the analysed area to approximately 0.03 cm on the short axis and line-scans with 0.02 cm step sizes (overlapping analysis areas) were taken across the standards in a direction parallel to the short axis of the slide and the short axis of the analysed area. Detailed information regarding ellipsometry data fitting is collected in the ESM.

Table 1 Summary of the LA-ICP-TOF-MS instrumental parameters for bioimaging analysis

Instrument parameters ICP-ToF-MS	
RF power	1550 W
Acquisition mode	Standard, no gas
Nebuliser gas flow	0.85 L min^{-1}
Sampling depth	3.3 mm
Laser parameters	
Acquisition mode	Imaging mode
Laser energy	4 J cm^{-2}
Laser spot size	18 μm
Repetition rate	50 Hz
Scan speed	500 μm s^{-1}
Helium flow rate	0.8 L min^{-1}

Results and discussion

Measuring droplet thickness using ellipsometry

Automating the preparation of calibration standards has the potential to minimise physical and chemical variation between individual standards and across batches. The current bioprinting method dispenses 55 gelatin droplets per microscope slide with an average weight of 0.95 ± 0.03 mg ($n = 10$ slides) per droplet before dehydration. The dried droplets have an average area of 5.90 ± 0.13 mm^2.

For this calibration strategy droplet thickness is a critical parameter to determine, not only to ensure the complete quantitative ablation of the droplets but also for being able to determine the mass of element present per pixel (ablation volume for each laser pulse) of the final image. Measuring film thickness of soft materials can be challenging. Commonly used approaches include profilometry,[31] or Atomic Force Microscopy (AFM), the later offering a spatial resolution between 0.1 and 1 nm depending on the material.[32,33] However, both are contact techniques, when measuring soft materials, like polymers, gels and biological tissue, contact artifacts can appear due to deformation of the sample by the probe, biasing results and increasing variability.[34,35] Other optical microscopy-based approaches are non-contact in nature but suffer from a lack of standardized calibration approaches.[25,36–38] In previous a previous study, droplet thickness was determined using fluorescence microscopy[26] whilst this technique provides measurement precision at the range of 0.3–0.5 μm,[39] the lack of

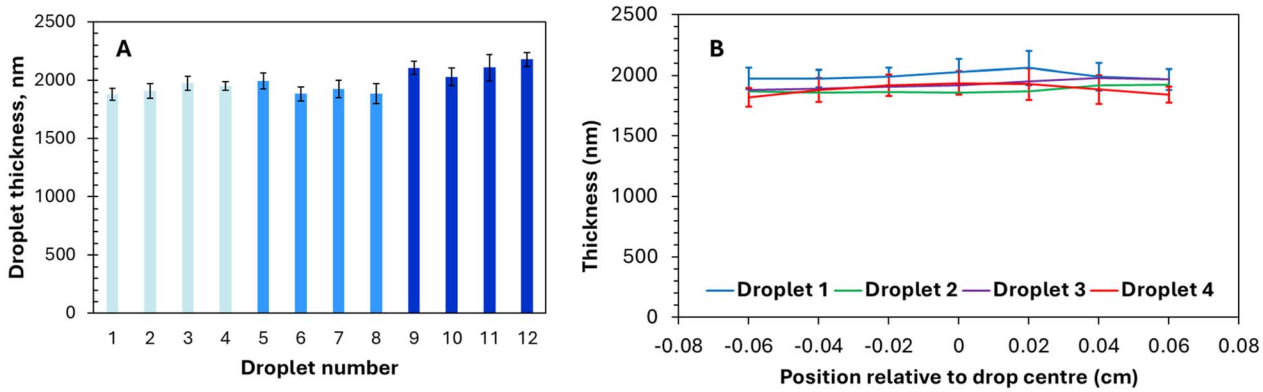

Fig. 1 Ellipsometry data (A) average thickness for $n = 12$ droplets, error bars show $\pm$ 2SD. Different colours were used to indicate measurements taken from different microscope slides and (B) linear profile for $n = 4$ droplets. Error bars showing thickness average variation across droplets 1 and 4.

a standardised approach for data processing or calibration of the instrument are remaining challenges.

In this work, ellipsometry was used to measure gelatin droplet thickness and variation both across and between droplets. Ellipsometry is an optical, non-contact technique, which eliminates the risk of sample deformation, particularly suitable for thickness measurement of soft materials[40,41] with reported accuracies around 1% for organic thin films.[42] Both droplet thickness and the overall droplet profile were characterised giving an average thickness of 1.98 ± 0.10 μm ($n = 12$) as shown in Fig. 1A. Ellipsometry measurements are taken as line scans across the diameter of the droplet and showed an overall variation of <8% (excluding the edge of each droplet), corresponding to <160 nm variation across the sample. These results show that, as well as a uniform average thickness, the dried droplets also have relatively flat profiles, ideal for quantitative ablation (Fig. 1B). Using ellipsometry to provide a metrological underpinning to the thickness measurement highlights the uniformity and usability of these calibration bioprinted standards.

Elemental homogeneity and printing repeatability

Achieving elemental homogeneity across the gelatin droplets is essential for resampling of the same droplet throughout an experiment and between different batches of analyses. This helps monitor signal drifts and sensitivity fluctuations that can occur during long bioimaging experiments.

Droplets were doped with Ti, Ce, Au, Th and U as tuning elements. As the sensitivity of the ICP-ToF-MS instrument increases at higher m/z, different concentrations were added to have similar intensity values for the different tuning elements. Ti was spiked at 400 mg kg^{-1}, Ce at 60 mg kg^{-1}, and Au, Th and

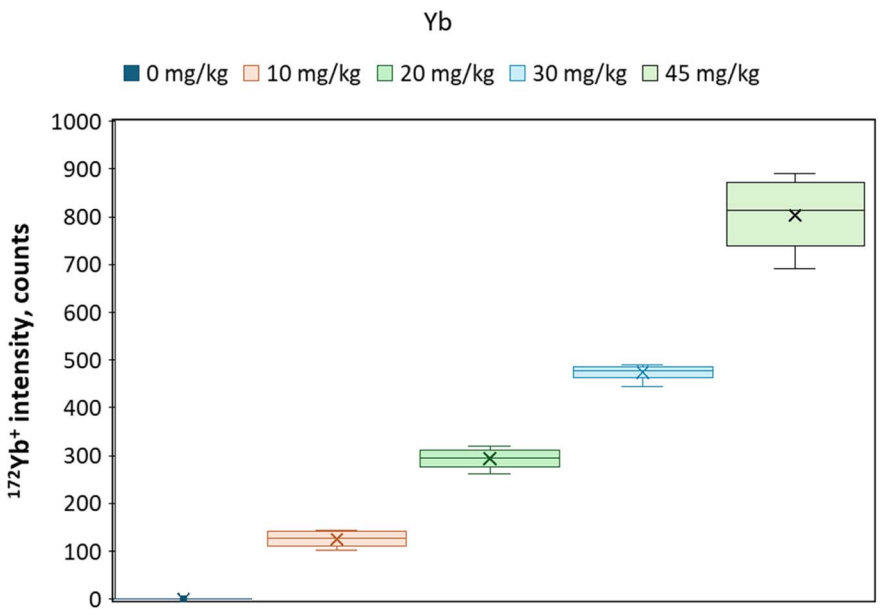

Fig. 2 Boxplots of $^{172}Yb^+$ intensity values across the different calibration levels. Each box represents the distribution of intensity values from ten equally sized sub-areas within the central region of the droplets. The boxes show the interquartile region (IQR), with the median indicated by the central line and the mean represented by a cross.

U at 30 mg kg^{-1}. To evaluate the performance of the proposed calibration workflow, gelatin solutions were also spiked with increasing amounts of Gd^{3+}/Yb^{3+} carbon dots (CDs) (0–90 mg kg^{-1} for Gd and 0–45 mg kg^{-1} for Yb). The different calibration levels and corresponding concentrations are collected in Table S2, only STD 3 contained the tuning elements in addition to Gd and Yb.

To evaluate the analyte homogeneity, elemental distribution maps were obtained by LA-ICP-MS (Fig. S4). Visual inspection of the elemental maps indicates a uniform distribution of the target elements across the droplet area, with no visual signs of coffee stain effect or gradients. To support this observation, the central area of the droplet was divided in 10 sub areas, each consisting in 5 lines (525 pixels), as seen in Fig. S5, boxplots were constructed to show elemental intensity distribution across the sub-areas within the droplet centre. Fig. 2 shows $^{172}Yb^+$ distribution at the different calibration levels. Overall, all calibration levels show symmetrical distributions as the mean and median intensities have similar values and balanced whisker lengths. Similar trends were observed for $^{158}Gd^+$ at all levels (Fig. S6), and for the single points of $^{48}Ti^+$, $^{140}Ce^+$ and $^{197}Au^+$ (Fig. S7).

Table 2 shows the relative standard deviation (RSD) values obtained for all investigated elements in a STD 3 droplet. RSD values ranged from 2.0 to 5.5% depending on the element. Batch-to-batch printing repeatability was also evaluated determining the between droplet RSD for 9 measured droplets. Such data is also shown in Table 2. The between droplet RSDs values are slightly larger compared to within droplet RSDs, but still below 7.2% for all tested elements, providing evidence that droplets/standards with repeatable elemental concentrations are obtained by the proposed printing workflow.

Instrumentation parameter optimisation/tuning with printed gelatin droplets: sensitivity, laser-induced fractionation and oxide formation

Daily tuning and checking the performance of a LA-ICPMS setup is usually the first step before analysing samples. For bioimaging experiments despite using matrix-matched calibration approaches, many authors still rely on NIST 61X series for tuning the instrument[10,17,43] due to the lack of a suitable alternative. The homogeneity of the analyte distribution across a relatively large ablation area of the bioprinted gelatin droplets and their reproducibility allows their use not only for calibration purposes but also for matrix-matched tuning of the LA-ICP-MS system.

Table 2 RSD from the mean element intensity values within subareas ($n = 10$) of the same droplet and between different droplets ($n = 9$)

Isotope	RSD within droplet (%)	RSD between droplets (%)
^{48}Ti	3.8	4.0
^{140}Ce	2.9	5.3
^{158}Gd	5.5	5.5
^{172}Yb	4.8	7.2
^{197}Au	2.9	5.8
^{232}Th	2.0	5.4
^{238}U	3.2	6.3

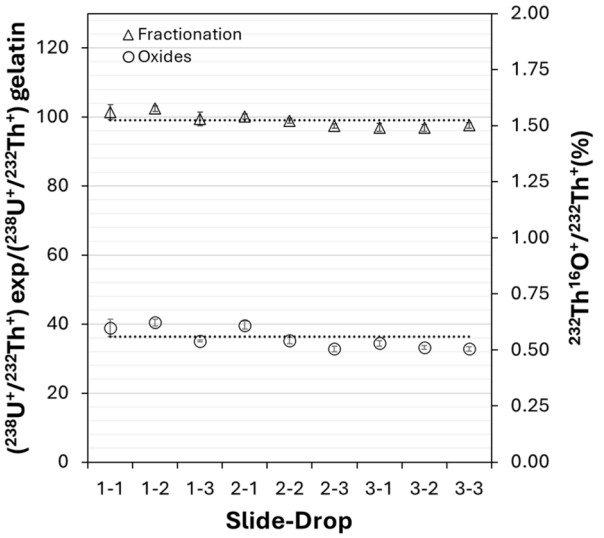

Fig. 3 Laser induced fractionation and oxide formation were monitored after tuning the LA system by measuring the $^{238}U^+/^{232}Th^+$ (triangles) and $^{232}Th^{16}O^+/^{232}Th^+$ (circles) ratios, respectively. The straight lines represent the average fractionation and oxide average values. Error bars show SD from the average.

Apart from elements used for calibration in quantitative bioimaging the gelatin droplets also contain, Ti, Ce and Au to assess sensitivity in the low, mid and high m/z ranges, as well as U and Th to evaluate laser-induced elemental fractionation and oxide formation. Having an all-in-one solution helps streamline the bioimaging workflow whilst also benefits users with laser systems of longer wavelength sources such as 266 nm.

The homogeneous analyte distribution in the gelatin droplets (see the elemental maps in Fig. S4) enables tuning of experimental parameters to maximise sensitivity as part of a daily tuning routine and to monitor performance changes day-to-day. Moreover, laser-induced elemental fractionation and oxide formation were evaluated by monitoring $^{238}U^+/^{232}Th^+$ and $^{232}Th^{16}O^+/^{232}Th^+$ ratios, respectively. Fig. 3 shows the values obtained for $^{238}U^+/^{232}Th^+$ and $^{232}Th^{16}O^+/^{232}Th^+$ ratios from 3 droplets across 3 microscope slides ($n = 9$). Note that the $^{238}U^+/^{232}Th^+$ ratio is normalized to the actual $^{238}U^+/^{232}Th^+$ ratio in the gelatin batch. Markers in the graph correspond to the average isotope intensity from 10 subareas within a droplet (each sub-area consisting in 5 lines) the error bars represent the standard deviation (SD) from the mean value. Average laser-induced fractionation of 99 ± 2% and oxide ratio of 0.55 ± 0.05% were reported. Moreover, the RSDs of these values was also determined within a droplet, <2.5% and 6.5% for the fractionation and oxide ratios, respectively. While the between droplet RSDs were 2% and 8%. These results, together with the elemental homogeneity discussed in previous sections, suggest that these gelatin standards are suitable for daily LA-ICP-MS tuning.

Assessing re-usability of gelatin standards

Lanthanide elements are key in LA-ICP-MS bioimaging experiments because of two main reasons. On the one hand, lanthanides are used in clinical treatments and as contrast agents.[44] Therefore, previous works use LA-ICP-MS to study lanthanide bioaccumulation in different tissues, from different models or real patients.[45,46] On the other hand, lanthanides are usually employed as markers for biomolecule imaging[47] and cell tagging.[48] From an analytical perspective, lanthanides also offer important advantages for ICP-TOF-MS analysis: due to their high m/z their detection is less affected by polyatomic interferences compared to lighter elements (*e.g.* Fe, Zn, Cu, *etc.*), they generate stable signals due to higher instrument sensitivity for heavier masses, and many of them are multi-isotopic, offering flexibility to select a less-interfered isotope for quantification. For these reasons, Gd and Yb were chosen as proof-of-concept elements to assess quantification performance in gelatin droplets.

Gelatin droplets with increasing Gd and Yb mass fractions were prepared and calibration curves constructed by averaging the element intensities from 3 droplets per calibration level, as seen in Fig. 4. A good linear fit was found for the two elements, with the coefficient of determination (R^2) > 0.99 in both cases. Limits of detection (LoD) were calculated as three times the standard deviation of the residuals of the calibration curves divided by the slope, and they were 5.4 and 1.0 mg kg^{-1} of Gd and Yb in the dry gelatin, respectively.

As mentioned earlier, for previously proposed automated calibration approaches, it was necessary to ablate the entire calibration standard droplet to enable quantification.[21,26] The newly bioprinted gelatin standards proposed in this work show a potential reusability based on their micro-scale homogeneity combined with their relatively large area (~6 mm^2), adding benefits to quantitative strategies for bioimaging analysis.

The minimum area that needs to be ablated per droplet to achieve elemental data that is representative of the entire droplet was investigated. Reducing the size of ablated area offers the benefit of both saving analysis time and reducing droplet destruction. However, there is a trade- off between using smaller ablated areas and minimising the error associated with the quantitative data.

Fig. 5 shows three calibration graphs for Gd produced by averaging the signal from 1, 5, or 50 lines (105 pixels per line) per mass fraction level. The full data set (3 replicas per calibration) is collected in Table S3. It is important to note that although the error associated with individual calibration points increases when decreasing the number of ablated lines (7%, 22% and 44% for 50, 5 and 1 lines), the linearity of the curve is maintained (R^2 > 0.99) and the slope varies by less than 1.2%. These results suggest the user can select a number of lines per standard in each experiment, balancing analysis time, associated error, and the number of lines available for resampling. For example, in experiments where differences between sample groups are expected to exceed 50%, analysing only one line per calibration point could be sufficient.

Standard stability

The impact of long-term storage conditions and shipping on the stability of the produced standards was also studied. Printed microscope slides were stored in the dark under controlled conditions (20 ± 2 °C and 50 ± 5% humidity) in a microscope slide box. A storage stability test was carried out by measuring the average elemental intensities and RSDs within a STD 3 droplet (for three independent droplets). Measurements were done at the time of printing (after 24 h drying period) and after three months of storage (analysing other droplets from the same microscope slide). Results summarised in Table 3 show that the average elemental sensitivities vary between the beginning of the experiment and the same batch measured three months after. This could be anticipated due to changes that usually occur in instrument tuning and sensitivity over time. The RSD values agreed between the two time points, providing a better indicator of unchanged homogeneity over the 3-month period. These RSDs are also in line with the

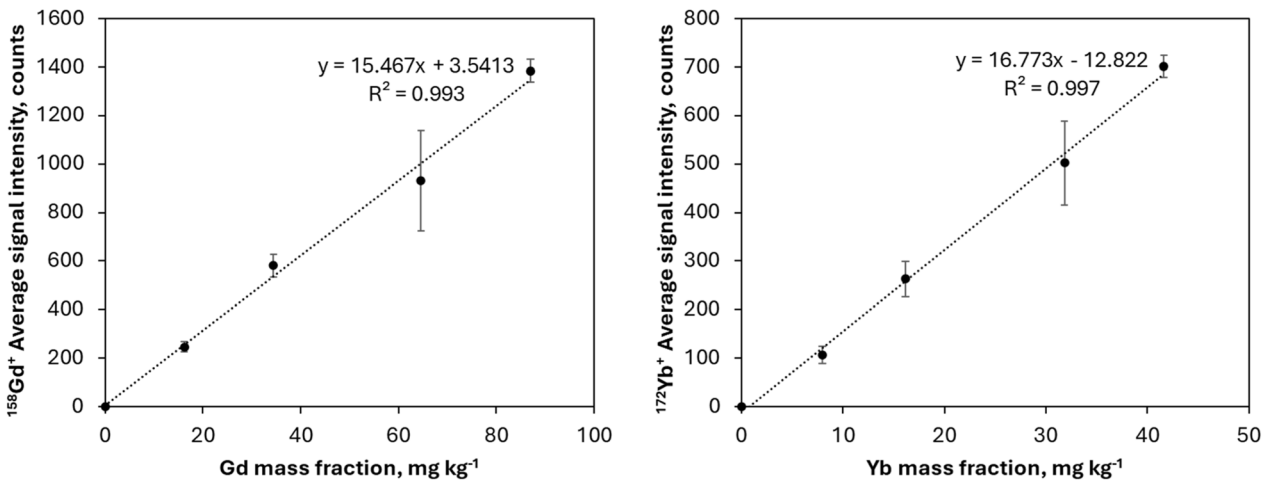

Fig. 4 Calibration curves obtained for Gd and Yb by averaging three whole droplets per calibration level. Error bars represent SD (n = 3) values from the mean value.

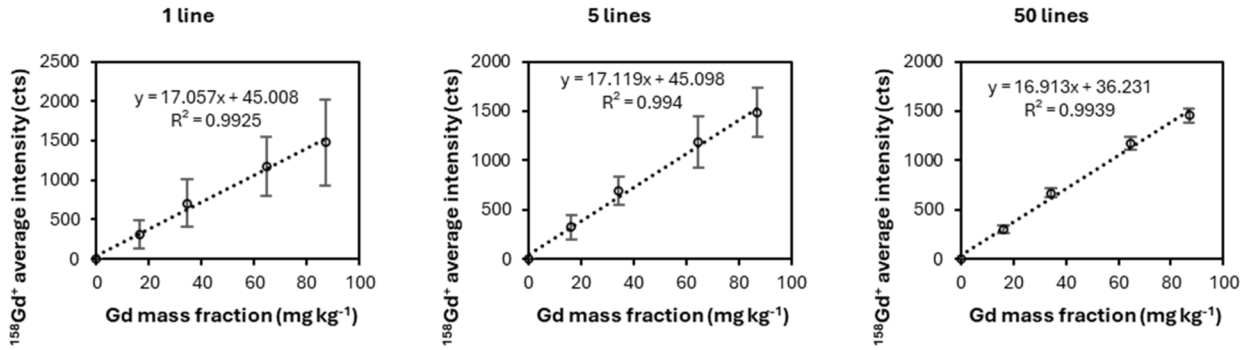

Fig. 5 Calibration curves for Gd obtained averaging (A) the central droplet line (B) five central lines or (C) 50 central lines. Error bars correspond to the expanded error ($k = 2$) of the average intensity, calculated as the standard deviation from the mean divided by the square root of the number of averaged lines.

Table 3 Stability data comparing average elemental intensities and within droplet RSD (from the centre of three droplets) and between freshly prepared standards and those stored for 3 and 12 months, the latter including shipping

	Freshly prepared		3-Months old		Shipped, 12 months-old	
Isotope	Average (cts)	RSD (%)	Average (cts)	RSD (%)	Average (cts)	RSD (%)
^{48}Ti	4613	8	5780	8	5975	4
^{140}Ce	1592	7	1340	7	1769	5
^{158}Gd	1652	4	710	5	1022	2
^{172}Yb	938	7	326	5	855	3
^{197}Au	2515	5	1333	8	2157	3

combination of the within and between droplet variabilities summarised in Table 2.

To prove that the elemental content does not leach over this time period and average intensity differences are a result of variation in instrument sensitivity, a droplet from a newly printed batch was also measured at the same time as the aged droplet (3-month older). As it can be seen in Table S4, average element intensities were comparable for a 3-month-old droplet and freshly prepared one, if measured on the same day.

To investigate the impact of shipping conditions on the standard stability, a printed microscope slide (from the initial batch of the stability study) was shipped (by air freight) inside a plastic microscope slide box and measured 12 months after printing in a different laboratory. The elemental distribution maps by LA-ICP-MS (Fig. S8) show no visual changes in elemental distribution compared to the fresh droplets (Fig. S4). As a different instrument was used to measure these droplets, absolute intensities cannot be directly compared, however, RSD values measured after shipping and 12-month storage were also in the same range as when the batch was freshly prepared, as it can be seen in Table 3. For all elements RSDs were <6% suggesting that shipping and long-term storage does not affect analyte homogeneity as long as the samples are stored under the conditions proposed as optimal in this work.

Conclusions

This work shows an improved workflow for the bioprinting, metrological characterization and use of multi-elemental gelatin droplets as calibration and tuning materials for LA-ICP-MS bioimaging.

The variation of droplet thickness (measured by ellipsometry), after printing and dehydration, was found below 8%. This combined with the intra- and inter-droplet elemental homogeneity obtained enable use of these standards for calibration without the need to ablate the whole droplet, enabling their use in multiple calibration batches or as quality control materials along a measurement session. Results show that even ablating one line per calibration level is representative of the whole gelatin droplet. However, the ablated area can be selected as a compromise between experimental time and acceptable measurement error according to the requirements of users' applications.

Preliminary data from long-term stability and shipping tests demonstrate the potential of this fit-for purpose production and characterisation workflow towards method evaluation and harmonisation through interlaboratory comparisons. However, to investigate the extent of application of these standards, ongoing studies involve further investigation of their stability under more extreme conditions (*e.g.* high/low temperatures and humidities).

Author contributions

K. B.: conceptualisation, methodology, investigation, formal analysis, validation, visualisation, writing – original draft, writing – review and editing. P. M. V.: conceptualization, formal analysis, investigation, writing-original draft. W. L.:

conceptualisation, methodology, investigation, formal analysis, writing – review and editing. A. S.: conceptualisation, methodology, investigation, formal analysis, writing – review and editing. H. G. I.: conceptualisation, methodology, resources, supervision, writing – review and editing, funding acquisition.

Conflicts of interest

There are no conflicts of interest to declare.

Data availability

The data underlying this article is found in the supplementary information (SI) and will be shared on reasonable request to the corresponding author. Supplementary information: describing LnQD synthesis, ellipsometry measurements, ICP-MS elemental analysis of the droplets, qualitative imagings and full data set for assesing the re-usability of standards. See DOI: **https://doi.org/10.1039/d5ja00350d**.

Acknowledgements

Authors would like to acknowledge David Douglas and Tristen Taylor from Elemental Scientific Lasers for their input in the shipping stability study and Christian Ward-Deitrich from National Measurement Laboratory (NML) for conducting total elemental analysis of the gelatin standards. Additionally, authors thank Ana Soldado and Jose M Costa-Fernandez from the University of Oviedo and Guillermo Redondo Fernandez from the NML for supplying the LnCDs used in this study. Authors would also like to acknowledge the UK Department of Science, Innovation and Technology (DSIT) for funding.

References

1 I. Basabe-Mendizabal, R. Maeda, S. Goderis, F. Vanhaecke and T. Van Acker, *Anal. Chem.*, 2025, **97**, 6481–6488.
2 K. Mervič, M. Šala and S. Theiner, *Trend. Anal. Chem.*, 2024, **172**, 117574.
3 N. Lv, K. Chen, Z. Bao, W. Kai, D. Lei and H. Yuan, *Atom. Spectros*, 2021, **42**, 51–61.
4 X. Liao, Z. Hu, T. Luo, W. Zhang, Y. Liu, K. Zong, I. Zhou and J. Zhang, *J. Anal. At. Spectrom.*, 2019, **34**, 1126–1134.
5 A. Limbeck, P. Galler, M. Bonta, G. Bauer, W. Nischkauer and F. Vanhaecke, *Anal. Bioanal. Chem.*, 2015, **407**, 6593–6617.
6 N. Miliszkiewicz, S. Walas and A. Tobiasz, *J. Anal. At. Spectrom.*, 2015, **30**, 327–338.
7 M. Martinez and M. Baudelet, *Anal. Bioanal. Chem.*, 2019, **36**, 421–427.
8 P. A. Doble, R. Gonzalez de Vega, D. P. Bishop, D. J. Hare and D. Clases, *Chem. Rev.*, 2021, **121**, 11769–11822.
9 N. Grijalba, A. Legrand, V. Holler and C. Bouvier-Capely, *Anal. Bioanal. Chem.*, 2020, **412**, 3113–3122.
10 J. O'Reilly, D. Douglas, J. Braybrook, P. W. So, E. Vergucht, J. Garrevoet, B. Vekemans, L. Vincze and H. Goenaga-Infante, *J. Anal. At. Spectrom.*, 2014, **29**, 1378–1384.
11 D. N. Douglas, J. O'Reilly, C. O'Connor, B. L. Sharp and H. Goenaga-Infante, *J. Anal. At. Spectrom.*, 2016, **31**, 270–279.
12 S. K. I. Funke, M. Sperling and U. Karst, *Anal. Chem.*, 2021, **93**, 15720–15727.
13 H. Pan, L. Feng, Y. Lui, Y. Han, J. Xiong and H. Li, *Trends Anal. Chem.*, 2022, **156**, 116710.
14 H. Sela, Z. Karpas, H. Cohen, Y. Zakon and Y. Zeiri, *Int. J. Mass Spectrom.*, 2011, **307**, 142–148.
15 D. J. Hare, J. Lear, D. Bishop, A. Beavis and P. A. Doble, *Anal. Methods*, 2013, **5**, 1915–1921.
16 C. Austin, D. Hare, T. Rawling, A. M. McDonagh and P. Doble, *J. Anal. At. Spectrom.*, 2010, **25**, 722–725.
17 C. Arnaudguilhem, M. Larroque, O. Sgarbura, D. Michau, F. Quenet, S. Carrère, B. Bouyssière and S. Mounicou, *Talanta*, 2021, **222**, 121537.
18 M. Šala, V. S. Šelih and J. T. van Elteren, *Analyst*, 2017, **142**, 3356–3359.
19 M. T. Westerhausen, T. E. Lockwood, R. Gonzalez de Vega, A. Röhnelt, D. P. Bishop, N. Cole, P. A. Doble and D. Clases, *Analyst*, 2019, **144**, 6881–6888.
20 P. Becker, T. Nauser, M. Wiggenhauser, B. Aeschlimann, E. Frossard and D. Günther, *Anal. Chem.*, 2024, **96**, 4952–4959.
21 R. Niehaus, M. Sperling and U. Karst, *J. Anal. At. Spectrom.*, 2015, **30**, 2056.
22 S. Theiner, E. Foels and G. Koellensperger, *Anal. Chim. Acta*, 2024, **1332**, 343345.
23 L. Labeyrie, G. S. Valverde, D. Michau, S. Fontagné-Dicharry and S. Mounicou, *Microchem. J.*, 2023, **194**, 109204.
24 B. Neumann, S. Hösl, K. Schwab, F. Theuring and N. Jakubowski, *J. Neurosci. Methods*, 2020, **334**, 108591.
25 A. Arakawa, N. Jakubowski, G. Koellensperger, S. Theiner, A. Schweikert, S. Flemig, D. Iwahata, H. Traub and T. Hirata, *Anal. Chem.*, 2019, **91**, 10197–10203.
26 K. Billimoria, Y. A. Diaz Fernandez, E. Andresen, I. Sorzabal-Bellido, G. Huelga-Suarez, D. Bartczak, C. Ortiz de Solorzano, U. Resch-Genger and H. Goenaga-Infante, *Metallomics*, 2022, **14**, mafc088.
27 A. Schweikert, S. Theiner, D. Wernitznig, A. Schoeberl, M. Schaier, S. Neumayer, B. K. Keppler and G. Koellensperger, *Anal. Bioanal. Chem.*, 2022, **414**, 485–495.
28 D. Metarapi, A. Schweikert, A. Jerše, M. Schaier, J. T. van Elteren, G. Koellensperger, S. Theiner and M. Šala, *Anal. Chem.*, 2023, **95**, 7804–7812.
29 G. Redondo-Fernandez, K. Billimoria, S. Cowen, D. Ojeda, D. Bartczak, A. Soldado, J. M. Costa-Fernandez and H. Goenaga Infante, *J. Anal. At. Spectrom.*, 2025, **40**, 1403–1410.
30 C. Paton, J. Hellstrom, B. Paul, J. Woodhead and J. Hergt, *J. Anal. At. Spectrom.*, 2011, **26**, 2508–2518.
31 M. Karthik, J. M. Gohil and A. K. Suresh, *Int. J. Hydrog. Energy*, 2017, **42**, 26464–26474.
32 C. Ton-That, A. G. Shard and R. H. Bradley, *Langmuir*, 2000, **16**, 2281–2284.
33 R. Garcia, *Chem. Soc. Rev.*, 2020, **49**, 5850–5884.
34 J. Giblin-Burnham, Y. Javanmardi, E. Moeendarbary and B. W. Hoogenboom, *Soft Matter*, 2024, **20**, 9483–9492.

35 Z. Li, U. Brand and T. Ahbe, *Meas. Sci. Technol.*, 2014, **25**, 044010.
36 G. Cox and C. J. R. Sheppard, *Micron*, 2001, **32**, 701–705.
37 Y. Zhou, K. K. H. Chan, T. Lai and S. Tang, *Biomed. Opt. Express*, 2013, **4**, 38–50.
38 (*a*) J. W. McLaren, C. B. Nau, J. C. Erie and W. M. Bourne, *Am. J. Ophtalmol.*, 2004, **137**, 1011–1020; (*b*) P. Sarder, S. Yazdanfar, W. J. Akers, R. Tang, G. P. Sudlow, C. Egbulefu and S. Achilefu, *J. Biomed. Opt.*, 2013, **18**, 106012.
39 S. Z. Bhutia, S. K. Sukumaran and D. K. Satapathy, *Langmuir*, 2024, **40**, 14153–14165.
40 D. Mitra, S. C. Bhattacharya and S. P. Moulik, *Biophys. Chem.*, 2009, **139**, 123–136.
41 A. Farahzadi, M. Beigmohamadi, P. Niyamakom, S. Kremers, N. Meyer, M. Heuken and M. Wuttig, *App. Surf. Sci.*, 2010, **256**, 6612–6619.
42 E. Valencia, B. Fernandez, M. Cruz-Alonso, M. Garcia, H. Gonzalez-Iglesias, M. T. Fernandez-Abedul and R. Pereiro, *J. Anal. At. Spectrom.*, 2020, **35**, 1868–1879.
43 R. H. Wallimann, A. Mehta, A. K. Mapanao, U. Köster, R. Kneuer, P. Schindler, N. P. van der Meulen, R. Schibli and C. Müller, *Eur. J. Nucl. Med. Mol. Imaging*, 2025, **52**, 1370–1382.
44 J. Saatz, H. Stryhanyuk, D. Vetterlein, N. Musat, M. Otto, T. Reemtsma, H. H. Richnow and B. Daus, *Environ. Poll.*, 2016, **216**, 245–252.
45 P. Bücker, H. Richter, A. Radbruch, M. Sperling, M. Brand, M. Holling, V. Van Marck, W. Paulus, A. Jeibmann and U. Karst, *J. Trace Elem. Med. Biol.*, 2021, **63**, 126665.
46 T. C. de Bang and S. Husted, *Trend. Anal. Chem.*, 2015, **72**, 45–52.
47 K. Löhr, H. Traub, A. J. Wanka, U. Panne and N. Jakubowski, *J. Anal. At. Spectrom.*, 2018, **33**, 1579–1587.
48 K. Löhr, H. Traub, A. J. Wanka, U. Panne and N. Jakubowski, *J. Anal. At. Spectrom.*, 2018, **33**, 1579–1587.